Title
Origins and Proliferative States of Human Oligodendrocyte Precursor Cells.

Journal
Cell, 182(3)

ISSN
0092-8674

Authors
Huang, Wei
Bhaduri, Aparna
Velmeshev, Dmitry
et al.

Publication Date
2020-08-01

DOI
10.1016/j.cell.2020.06.027

Peer reviewed

HHS Public Access

Author manuscript

Cell. Author manuscript; available in PMC 2021 August 06.

Published in final edited form as:

Cell. 2020 August 06; 182(3): 594–608.e11. doi:10.1016/j.cell.2020.06.027.

Origins and Proliferative States of Human Oligodendrocyte Precursor Cells

Wei Huang[1,2,7,*], **Aparna Bhaduri**[1,2,7], **Dmitry Velmeshev**[1,2], **Shaohui Wang**[1,2], **Li Wang**[1,2], **Catherine A. Rottkamp**[1,8], **Arturo Alvarez-Buylla**[1,3], **David H. Rowitch**[1,4,5,6], **Arnold R. Kriegstein**[1,2,9,*]

[1]The Eli and Edythe Broad Center of Regeneration Medicine and Stem Cell Research, University of California, San Francisco, San Francisco, CA 94143, USA

[2]Department of Neurology, University of California, San Francisco, San Francisco, CA 94143, USA

[3]Department of Neurological Surgery, University of California, San Francisco, San Francisco, CA 94143, USA

[4]Departments of Pediatrics and Neurosurgery, University of California, San Francisco, San Francisco, CA 94143, USA

[5]Department of Paediatrics, University of Cambridge, Cambridge CB2 0QQ, UK

[6]Wellcome-MRC Cambridge Stem Cell Institute, University of Cambridge, Cambridge CB2 0QQ, UK

[7]These authors contributed equally

[8]Present address: Department of Pediatrics, UC Davis Children's Hospital, Sacramento, CA 95817, USA

[9]Lead Contact

SUMMARY

Human cerebral cortex size and complexity has increased greatly during evolution. While increased progenitor diversity and enhanced proliferative potential play important roles in human neurogenesis and gray matter expansion, the mechanisms of human oligodendrogenesis and white matter expansion remain largely unknown. Here, we identify EGFR-expressing "Pre-OPCs" that originate from outer radial glial cells (oRGs) and undergo mitotic somal translocation (MST) during division. oRG-derived Pre-OPCs provide an additional source of human cortical

*Correspondence: wei.huang@ucsf.edu (W.H.), arnold.kriegstein@ucsf.edu (A.R.K.).

AUTHOR CONTRIBUTIONS

A.R.K., W.H., A.A.-B., and D.H.R. conceived and supervised the project. W.H. designed and performed all the functional experiments. A.B. and D.V. performed bioinformatics analysis. S.W. collected tissue samples and made the frozen sections for immunohistochemistry. L.W. performed shRNA efficiency test and FACS-based antibody specificity test. C.A.R. initiated this project. W.H., A.R.K., and D.H.R. wrote the manuscript with the input from all authors.

DECLARATION OF INTERESTS

A.R.K. is a co-founder and board member of Neurona Therapeutics.

SUPPLEMENTAL INFORMATION

Supplemental Information can be found online at https://doi.org/10.1016/j.cell.2020.06.027.

oligodendrocyte precursor cells (OPCs) and define a lineage trajectory. We further show that human OPCs undergo consecutive symmetric divisions to exponentially increase the progenitor pool size. Additionally, we find that the OPC-enriched gene, *PCDH15,* mediates daughter cell repulsion and facilitates proliferation. These findings indicate properties of OPC derivation, proliferation, and dispersion important for human white matter expansion and myelination.

In Brief

The properties of human oligodendrocyte precursor cell derivation, proliferation, and dispersion are explored and provide insight into white matter expansion and myelination in the brain.

Graphical Abstract

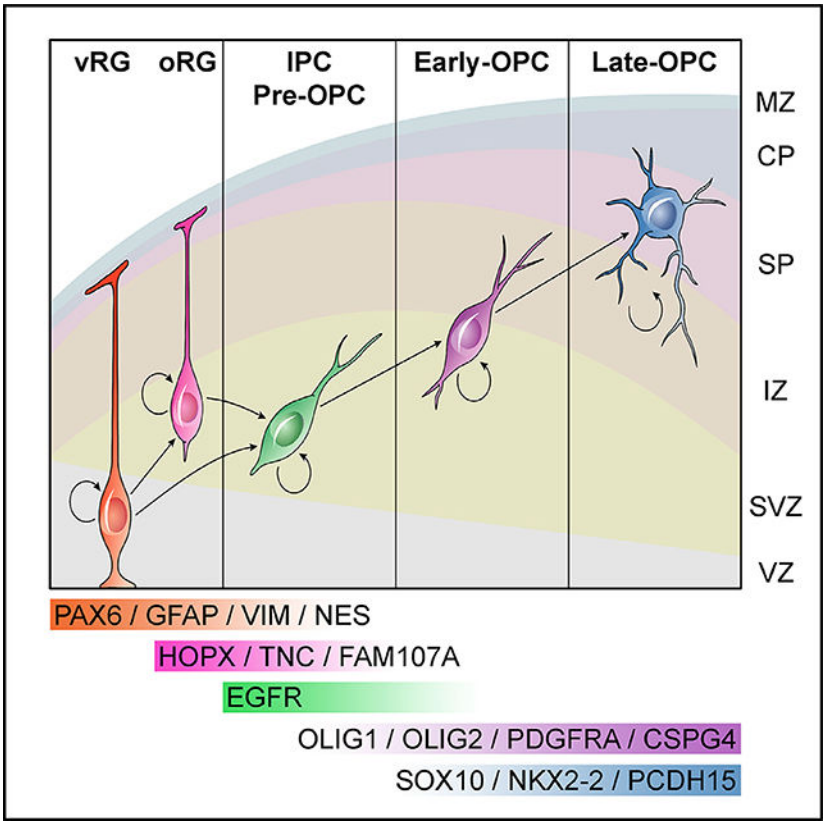

INTRODUCTION

Human cerebral white matter has enlarged dramatically during evolution, owing to increased axon fibers and glial cells. Myelinating oligodendrocytes, which first appear in jawed vertebrates, promote greatly enhanced saltatory conduction along axons of the central nervous system (Zhang and Sejnowski, 2000; Freeman and Rowitch, 2013; Simons and Nave, 2015). While much insight into oligodendrocyte development has been gained from animal studies (Fancy et al., 2011; Bergles and Richardson, 2015; Emery and Lu, 2015), a key challenge is to understand how oligodendrocytes populate human white matter, which is ~3,000-fold larger than its rodent counterpart.

In rodent forebrain, oligodendrocytes arise from the differentiation of oligodendrocyte precursor cells (OPCs) in temporally distinct waves from the ganglionic eminences (GE) and cortical ventricular zone (VZ) (Kessaris et al., 2006; Warf et al., 1991; Pringle and Richardson, 1993; Cai et al., 2005; Fogarty et al., 2005; Vallstedt et al., 2005), processes that appear conserved in humans (Jakovcevski and Zecevic, 2005; Rakic and Zecevic, 2003; Mo and Zecevic, 2009). Humans additionally develop an enlarged cortical germinal zone called the outer subventricular zone (OSVZ) (Smart et al., 2002; Zecevic et al., 2005; Fish et al., 2008), populated with outer radial glia (oRG) (Hansen et al., 2010; Fietz et al., 2010). Although diverse progenitors of the OSVZ contribute to enhanced neurogenesis (Lui et al., 2011; Betizeau et al., 2013; Nonako-Kinoshita et al., 2013), human OPC production from the cortical OSVZ and mechanisms regulating their proliferation and expansion are poorly understood.

Here, we investigate the trajectory of human cortical OPC production. Combining single-cell RNA sequencing (scRNA-seq) with functional studies, we identify a type of gliogenic intermediate progenitor cell (IPC) ($EGFR^+$ Pre-OPC) with diminutive mitotic somal translocation (MST) behavior. We also find that oRG cells provide an extra source of OPC production in the human cortex. Furthermore, we observe high levels of OPC proliferation and describe a repulsive behavior between OPC daughter cells mediated by the OPC-enriched gene *PCDH15.* The latter serves to avoid local OPC accumulation and facilitate OPC proliferation. These findings highlight an oligodendrocyte lineage in the human brain with enhanced precursor proliferation and a mechanism for cell dispersion, deepening our understanding of human oligodendrogenesis and white matter expansion.

RESULTS

Transcriptional Profiles of OPCs in the Developing Human Cortex

In order to study the diversity and developmental trajectories of human OPCs, we first consulted a single-cell transcriptomic atlas generated from 48 individuals in the late first and second trimester of gestation (Figures 1A and 1B) that comprised neural progenitor cells (NPCs), IPCs, neurons, macroglia, microglia, and endothelial cells (Nowakowski et al., 2017). However, we found only that 40 of the 4,261 unbiased captured cells were OPCs that expressed PDGFRA (Figure 1B), possibly due to low abundance and high fragility. While fluorescence-activated cell sorting (FACS) of labeled transgenic mouse OPCs (e.g., *PDGFRA*-H2B-*GFP*) has been used for scRNA-seq (Marques et al., 2016, 2018), we purified human embryonic OPCs by immunopanning (Dugas and Emery, 2013; Barres, 2014) (Figure 1A). Cortical cells were dissociated from nine brain samples at GW20–GW24, and cells expressing PDGFRA were collected using PDGFRA-antibody-coated Petri dishes. Immunostaining showed that most purified cells were $PDGFRA^+NKX2–2^+$, and scRNA-seq confirmed *PDGFRA* mRNA expression (Figure 1C). When we combined these PDGFRA-immunopanned cells with our previous 4,261 unbiased captured cells and clustered them by principal-component analysis (PCA) and Louvain-Jaccard clustering, a total of 980 high-quality cells were characterized as OPCs (Figure 1D). Differential gene expression analysis showed that these cells expressed conventional OPC genes *OLIG1, OLIG2, PDGFRA, NKX2–2, SOX10, S100B,* and *APOD* (Figure 1E). Conversely, they did

not express neuronal lineage genes *EOMES, PPP1R17, NEUROD2,* or *NEUROD6,* and separated from clusters of IPCs, excitatory neurons (EN), and interneurons (INs) (Figure 1F).

The OPCs clustered into four groups (clusters 14, 2, 20, and 11). Metadata annotation showed that cortical OPCs acquired by unbiased-capture were comparable to OPCs enriched by PDGFRA immunopanning, and major groups were composed of cells from multiple individuals (Figure 2A), indicating minimal technical and/or batch artifacts. Cluster 20 included the largest number of PDGFRA-immunopanned cells (Figure 2A), and cluster 2 was similar, suggesting these two clusters might reflect OPCs at different maturation states. In contrast, cluster 11 expressed cell-cycling genes *MKI67, ASPM, TOP2A,* and *CDK1,* suggesting that these OPCs were actively dividing (Figure 2B). Metadata analysis showed that cluster 14 was mainly composed of cells micro-dissected from the cortical germinal zone (Cortex-VZ/SVZ) (Figure 2A). Cluster 14 expressed low levels of NPC genes, including *GFAP, VIM, NES, HES1, NOTCH2,* and *EGFR,* as well as oligodendrocyte lineage genes *OLIG1, OLIG2,* and *PDGFRA;* the later stage OPC genes like *NKX2–2, SOX10,* and *APOD* were not expressed (Figure 2B). Similarity analysis indicated that cluster 14 was closely related to both NPCs and OPCs (Figure 2C), suggesting a transitional "Pre-OPC" stage from multi-potent NPCs to lineage committed OPCs. This was supported by a trajectory reconstruction based upon our scRNA-seq using monocle (Trapnell et al., 2014; Qiu et al., 2017) (Figures 2D and 2E). According to the pseudo-lineage tree, *VIM*-expressing NPCs could generate Pre-OPCs or *EOMES*-expressing IPCs that further differentiate into *NEUROD6*-expressing neurons. Feature plots showed NPC genes like *VIM* and *GFAP* were downregulated upon lineage commitment, while OPC genes like *PDGFRA* and *APOD* were upregulated. Together, our scRNA-seq analysis suggested a local intermediate progenitor source of Pre-OPCs supporting OPC generation in the human cortex.

EGFR Expression Marks Intermediate Pre-OPCs

While prior scRNA-seq analysis has indicated that mouse oligodendrocytes progress through various stages of differentiation (Marques et al., 2016 and 2018), progenitor types that generate OPCs prior to lineage commitment remain unclear. We first used immunohistochemistry to characterize OPCs in fixed human cortical sections and found that $PDGFRA^+OLIG2^+$ OPCs were present in low numbers across all cortical laminae and were distributed radially from VZ to the cortical plate (CP) during middle to late stages of neurogenesis (GW16 and GW18). The number of OPCs increased dramatically after GW20 and continued to increase at GW24, the latest age we studied (Figures S1A and S1B).

We then evaluated cluster 14 Pre-OPCs by co-staining OPC and NPC markers in GW20–24 tissue. While most $PDGFRA^+OLIG2^+$ OPCs did not express NPC markers, >10% of OPCs expressing low levels of PDGFRA and OLIG2 co-expressed NPC markers NES, GFAP, VIM, and EGFR, confirming the NPC signature (Figure 3A). $EGFR^+PDGFRA^+$ cells also expressed OPC markers OLIG1 and NG2 and had bipolar morphology typical of OPCs (Figure 3A). Distribution analysis showed that most $EGFR^+PDGFRA^+OLIG2^+$ cells were located in the OSVZ, though some were also present in the inner subventricular zone (ISVZ)

and intermediate zone (IZ) (Figure S1C). Considering their NPC and OPC marker co-expression, immature bipolar morphology, and germinal zone location, we reasoned that these cells represent a transitional stage from NPCs to OPCs, consistent with our scRNA-seq data (Figure 2).

In normal development, EGFR signaling regulates oligodendrogenesis and myelination in both juvenile and adult mice (Aguirre et al., 2007). Differential gene analysis based on scRNA-seq showed that EGFR was enriched in cluster 14 and expressed in a subpopulation of NPCs (Figures 2B and 2E). At the onset of gliogenesis (GW20–24), we found a large population of $EGFR^{+}OLIG2^{+}$ cells in cortical germinal zones. These cells were present at low abundance at GW16–18 but increased dramatically between GW20 and 24 (Figure S1D), coinciding with OPC generation (Figure S1B). They were highly proliferative, with 50% expressing KI67, and were mainly located in the OSVZ (Figure S1D). We did not observe *KI67* expression in cluster 14 in our scRNA-seq data (Figure 2B) because the abundance of cell-cycling genes drove the proliferative $EGFR^{+}OLIG2^{+}$ cells into cluster 11, which included both proliferative Pre-OPCs ($EGFR^{+}$) and dividing OPCs ($EGFR^{-}$). Unlike oRGs that exhibit a long radial process, EGFR-expressing cells were found randomly oriented in the germinal zone, being vertical, oblique, or even horizontal to the ventricular surface. Most $EGFR^{+}OLIG2^{+}$ cells did not express pS6 (Figure 3B), an oRG marker and a canonical readout of activated mTOR signaling (Nowakowski et al., 2017). Conversely, most $TNC^{+}SOX2^{+}$ oRGs in the OSVZ did not express EGFR (Pollen et al., 2015) (Figure 3B). These results suggest that EGFR labels a population of progenitor cells in the OSVZ distinct from oRGs. Moreover, $EGFR^{+}OLIG2^{+}$ cells were $EOMES^{-}$ and $PPP1R17^{-}$, suggesting a lineage separation between oligodendrocytes and neurons (Figure 3B). Together these findings indicate that EGFR expression marks a pre-OPC in human OSVZ.

EGFR-Expressing OSVZ Progenitors Generate OPCs

We next tested whether the EGFR-expressing progenitors of human OSVZ could generate OPCs. Cells were dissociated from micro-dissected OSVZ at GW20–24. OPCs were depleted by two sequential rounds of PDGFRA and O4 immunopanning to ensure that any OPCs detected arose from precursor cells and not by OPC self-renewal (Figure 3C). Cells were further purified through positive selection by EGFR immunopanning. Such EGFR-expressing non-OPC cells were cultured in EGF-containing medium for 2 days and then in PDGF-containing medium for 5 days. Preps were fixed at 2 days *in vitro* (DIV2) or 7 days *in vitro* (DIV7). At DIV2, 90%–96% of the cells were $EGFR^{+}$ and 23% were $OLIG2^{+}$, but none were $NG2^{+}$, $PDGFRA^{+}$, or $NKX2–2^{+}$, consistent with OPC depletion (Figure 3C). In contrast, by DIV7, the percentage of $EGFR^{+}$ cells was 40%–48%, while the percentage of $OLIG2^{+}$, $PDGFRA^{+}$, $NG2^{+}$, and $NKX2–2^{+}$ cells had increased to 35%, 35%, 36%, and 28%, respectively (Figure 3C). Reduction of EGFR-expressing progenitor cells accompanied the generation of OPCs, providing evidence that $EGFR^{+}$ progenitors in the human OSVZ have the ability to produce OPCs.

We reasoned that if the EGFR-expressing cells were progenitors of OPCs, then manipulation of the EGFR signaling pathway might affect EGFR-expressing cell proliferation and ultimately change OPC production. To test this possibility, we cultured human brain slices at

GW20–24 and treated adjacent slices with EGF, or with the EGFR inhibitors, Iressa, AG1478, or PD153035. Slices were incubated with bromodeoxyuridine (BrdU) for 12 hr before fixation at DIV7. In comparison with DMSO-treated control slices, EGF treatment resulted in dose-dependent increased in the numbers of both $OLIG2^+KI67^+$ and $NKX2–2^+BrdU^+$ cells; conversely, both populations were reduced significantly by EGFR inhibitor treatment (Figure 3D). This result combined with the differentiation assay supports the concept of local generation of OPCs from EGFR-expressing progenitors in late second trimester human cortex.

oRGs Are an Additional Source of OPCs in the Developing Human Brain

Neurogenic oRGs are a subtype of radial glia found in the primate OSVZ that are rare in rodents and are thought to contribute to gray matter expansion (Hansen et al., 2010; Fietz et al., 2010). However, the mechanisms underlying white matter expansion remain unknown, and whether oRGs are involved in human gliogenesis has not been fully demonstrated. The findings above show that, while VZ contains few $PDGFRA^+OLIG2^+$ cells, both $PDGFRA^+OLIG2^+KI67^+$ OPCs and $EGFR^+OLIG2^+KI67^+$ Pre-OPCs are mainly located in the OSVZ (Figures S1B and S1D). Through differential gene expression analysis of scRNA-seq data of human OPCs, we found that the Pre-OPC cluster also expressed the oRG genes *PTPRZ1*, TNC, *MOXD1*, *HOPX,* and *FAM107A* (Pollen et al., 2015) (Figure 2B), suggesting that oRGs might generate Pre-OPCs.

Immunohistochemistry of fixed cortical sections between GW20 and GW24 showed that fewer than 2% of $PDGFRA^+OLIG2^+$ cells co-expressed the oRG markers, HOPX, PTPRZ1, TNC, and pS6 (Figure S2A). These cells were far less numerous than contemporaneous $EGFR^+PDGFRA^+OLIG2^+$ cells. We already showed that most $EGFR^+OLIG2^+$ cells did not express the active mTOR readout and oRG marker pS6, and most TNC^+Sox2^+ oRGs also did not express EGFR (Figure 3B), but we found that about 10% of $PTPRZ1^+SOX2^+$ oRGs in the OSVZ expressed EGFR, and nearly 20% of $EGFR^+OLIG2^+$ progenitors were co-labeled with the oRG marker HOPX (Figures S1E and S2B). This indicated that the expression time windows of different oRG markers might be slightly different from one another, and that some oRG progeny still retain oRG marker expression, enabling lineage tracing and trajectory reconstruction. Distribution analysis of cortical staining at GW22 revealed that the $HOPX^+EGFR^+OLIG2^+$ cells were mainly located in the OSVZ (Figure S1E), suggesting that oRGs might be precursors of EGFR-expressing intermediate progenitors that produce OPCs. This concept is supported by our lineage trajectory reconstruction in which $HOPX^+TNC^+$ oRGs give rise to VIM^+EGFR^+ progenitors that further branch into $EOMES^+$ neurogenic IPCs or $OLIG2^+$ Pre-OPCs (Figures 2D and 2E).

To directly test whether HOPX-expressing oRGs could generate OPCs, we micro-dissected OSVZ at GW20–24. Two sequential rounds of negative selection of ($PDGFRA^+O4$) and EGFR immunopanning were performed in order to deplete both OPCs and Pre-OPCs in the cell suspension (Figure S2C). oRGs were further enriched through positive selection by LIFR immunopanning (Pollen et al., 2015) and expanded in LIF-containing medium for 2 days followed by EGF- and PDGF-containing medium for another 8 days. As shown (Figure S2C), at DIV2 around 90% of the cells expressed SOX2, and of these >90% co-expressed

GFAP$^+$HOPX$^+$, indicating oRG identity (Figure S2C). In contrast, at DIV10, the percentage of SOX2$^+$ cells decreased to 82%, and the percentage of GFAP$^+$HOPX$^+$ co-expression decreased to 50%. Meanwhile, the percentage of EGFR$^+$ cells increased to 44%, and the percentage of PDGFRA$^+$OLIG2$^+$ cells increased to 17% (Figure S2C). These findings suggested LIFR-antibody-enriched oRGs are able to produce OPCs.

The observation that nearly all the PDGFRA$^+$OLIG2$^+$ OPCs generated at DIV10 also expressed EGFR indicates that oRGs generate OPCs through EGFR-expressing Pre-OPCs, consistent with the lineage reconstruction based on scRNA-seq analysis (Figures 2D and 2E). This differentiation assay combined with scRNA-seq and immunohistochemistry data indicate that a population of late second trimester oRGs act as neural progenitors for oligodendrogenesis. Our results suggest that besides originating from ventricular radial glia (vRG) present in both rodent and primate brain, the large abundance of oRGs in the developing human brain provides an extra source of OPC production not found in rodents, that could enhance oligodendrocyte generation and boost myelination to match demands arising from increased neurogenesis in the human brain.

Division Dynamics of EGFR-Expressing Progenitors in the OSVZ

We next studied the proliferative behavior of Pre-OPCs compared to oRGs and OPCs by time-lapse imaging. Due to the diversity of progenitors in the germinal zones at late second trimester and the lack of genetic tools to specifically label OPCs, EGFR-expressing IPCs, or oRGs, we dissociated cortical cells from OSVZ at GW20–24 and performed immunopanning to selectively enrich specific progenitor populations through sequential positive selection with PDGFRA, EGFR, and LIFR antibodies (Figure 4A). We labeled the enriched progenitor types with *CMV-GFP* adenovirus, transplanted the virus-labeled progenitors back into OSVZ of adjacent slices, and cultured the brain slices without growth factors (Figure 4B).

To validate the identity of enriched cells, we performed 10X scRNA-seq of the immunopanned cells prior to virus infection and transplantation (Figure S3A). Most LIFR-panned cells expressed *LIFR,* and the major clusters show enrichment for *GFAP, PAX6, HOPX,* and *PTPRZ1,* indicating oRG identity; the remaining non-oRG clusters were astrocytes, LIFR-expressing microglia, or newborn neurons (Figure S3A and S3B). Similarly, most EGFR-panned cells expressed *EGFR* and were enriched for *NES, SOX2,* and *VIM,* consistent with immunostaining in fixed brain slices and indicating progenitor identity (Figures S3A and S3B). Most PDGFRA-panned cells expressed *PDGFRA,* and the major clusters were also enriched for *OLIG1, OLIG2, NKX2–2,* and *SOX10,* reflecting OPC identity (Figures S3A and S3B).

Video frames were captured every 35 min for 72 hr (DIV3–6) and GFP-labeled progenitors were observed to migrate on cultured brain slices and divide. Interestingly, most LIFR-panned cells acquired a long radial fiber after transplantation, characteristic of radial glia (Figure S3C). The remaining non-radial cells might represent off-target cells or progeny generated by oRGs during the 3 days required for cell recovery and virus expression. Both EGFR- and PDGFRA-panned cells exhibited bipolar morphology but did not show any orientation preference (Figure S3C). Radial cells enriched by LIFR-panning MST (Figure

4C; Video S1), a “jump-and-divide” behavior of oRGs (Hansen et al., 2010; Noctor et al., 2001; Betizeau et al., 2013; Subramanian et al., 2017). In contrast, PDGFRA-panned cells rounded up in place to divide (Figure 4C).

While most EGFR-panned cells also jumped and divided, the distance of MST was much smaller than oRGs (Figure 4C; Video S2). Both EGFR-panned daughter cells regrew processes, resembling OPCs (Figure 4C). After division, daughter cells of both oRGs and EGFR-panned cells stayed close to each other, while the daughter cells of OPCs rapidly migrated away from each other. Figures 4D and 4E show the quantification of MST distance and daughter cell distance from 30 samples of each type of cell. Thus, EGFR-expressing cells exhibit their own proliferation pattern but with features resembling a combination of oRG and OPC behavior. Lineage reconstruction by monocle based on scRNA-seq data of unbiased captured cells (Bhaduri et al., 2020) also supports the developmental trajectory from oRG to EGFR-expressing IPC to OPC (Figure S3D). We incubated brain slices with either EGF or the EGFR inhibitor, Iressa, after EGFR panning, virus labeling, and cell transplantation. When post-stained for NKX2–2 and GFP at DIV7 and compared with DMSO-treated control slices, EGF treatment increased while Iressa treatment decreased OPC production from EGFR-panned cells (Figure 4E), indicating an essential role of EGFR-expressing cells in OPC generation.

Transient Amplification of Human OPCs in the Late Second Trimester

We next focused on the proliferative ability of OPCs by studying the time-lapse image data generated above. An average of 20 cells were found to divide within a single visual field, and 42 cells were observed to undergo two rounds of division among all 24 visual fields. Figure 5A shows an example of an OPC that divided to generate two daughter cells, both of which divided again at similar time points to produce four granddaughter cells (Video S3). These observations suggest that OPCs undergo frequent repeated symmetric divisions to exponentially increase the progenitor cell pool. This differs from observations of the mouse brain at comparable neonatal ages, where *NG2*-expressing OPCs divide only once in a 5-day period to generate two daughter cells that continue to express NG2 for several days before one or both differentiate into oligodendrocytes (Zhu et al., 2011; Hill et al., 2014).

Robust OPC migratory behavior resulted in daughter cells often leaving the field of vision, making it difficult to quantitatively analyze the percentage of continuously dividing OPCs by live imaging. Thus, we performed thymidine analog labeling to quantify cell divisions (Figure 5B). We labeled PDGFRA-panned OPCs with *CMV-GFP* adenovirus prior to transplantation into cultured brain slices, incubated brain slices with the thymidine analog, chlorodeoxyuridine (CldU), for 12 hr followed by 24 hr without thymidine analog, and then another 12 hr exposure to the thymidine analog, iododeoxyuridine (IdU), followed by 24 hr without thymidine analog prior to fixation. This was intended to differentially label successive rounds of cell division and to avoid CldU and IdU incorporation into cells during the same S-phase, as our time-lapse imaging indicated that the time interval between two rounds of division was about 36 hr. After fixation we stained the brain slices with OLIG2 that labeled 95% of GFP cells, indicating a high efficiency of OPC enrichment. Approximately 35% of GFP^+OLIG2^+ cells were either $CldU^+$ or IdU^+, while 8% of GFP

$^{+}$OLIG2^{+} cells were CldU^{+}IdU^{+}, indicating two rounds of cell division after OPC commitment (Figure 5B). Considering that cells were exposed to the thymidine analog for only 1/3 of their cell cycle and that the cycling OPCs were unsynchronized, the proportion of cycling cells should be triple the thymidine analog-labeled number. Thus, both time-lapse imaging and thymidine analog labeling suggest near continuous division of OPCs in the developing human brain. These results support the concept that during human cortical development, OPCs undergo a prolonged period of proliferation before differentiation and thus act as transit amplifying cells to greatly increase the progenitor pool through symmetric division.

OPC-Enriched *PCDH15* Mediates Daughter Cell Separation and Dispersal after Division

Previous studies and our time-lapse imaging of LIFR- and EGFR-panned cells show that the daughter cells of progenitors usually stay in contact or close to each other long after division (Hansen et al., 2010; Betizeau et al., 2013; Subramanian et al., 2017). However, our time-lapse imaging of PDGFRA-panned cells revealed an unusual behavior. Immediately following OPC division, the newly generated daughter cells appeared to repel each other and migrate rapidly in opposite directions (Figure 4C). We reasoned that this behavior might serve to ensure broad distribution of OPCs across the developing cortex.

To explore the mechanism underlying repulsion, we first compared the RNA profiles of dividing OPCs with other dividing cortical progenitors whose daughters do not repel each other after division (RGs and IPCs). The list of differentially expressed genes included the cell-surface molecules *PCDH15* and *DSCAM,* which ranked high among OPC-enriched genes (Figures 6A and 6B). DSCAM belongs to the immunoglobulin (Ig) superfamily of cell adhesion molecules. It promotes repulsion between neurites and mediates tiling between neurons (Fuerst et al., 2008; Hattori et al., 2008). PCDH15 is a member of the protocadherin superfamily. Although the function of PCDH15 in OPC development is unknown, other members of the protocadherin family have been reported to mediate dendritic self-avoidance (Lyfebvre et al., 2012).

In order to study the function of PCDH15 and DSCAM in OPCs, we used knockdown of *PCDH15* or *DSCAM* by short hairpin RNA (shRNA) lentivirus (Figures S4A and S4B). We performed PDGFRA immunopanning to enrich human OPCs at GW20–24 and infected them with either PCDH15-shRNA-GFP or *DSCAM*-shRNA-*GFP* lentivirus. We transplanted the virus-infected OPCs into cultured cortical slices and performed time-lapse imaging at DIV3–6. The scramble-control exhibited similar behavior to that observed in the *CMV-GFP* adenovirus-labeled cells (Figures 4C and 5A; Video S3); namely, OPC daughter cells repelled each other and migrated rapidly in opposite directions (Figure 6C; Video S4). In contrast, the *PCDH15*-shRNA-infected daughter cells remained in contact with or close to each other following division, often for many hours (Figure 6C; Video S5). Quantitative analysis of daughter cell distances from one another showed dramatic increases at 5, to 10, and 15 hr after OPC division in the scramble control, while the separation between daughter cells was much smaller in *PCDH15*-shRNA at the same time points, with no obvious increase between different time points (Figure 6D), indicating significant inhibition of daughter cell dispersion after *PCDH15* knockdown. Statistical analysis of the migration

speed before division shows no obvious difference between scramble-control and *PCDH15*-shRNA (Figure 6E), indicating that the inhibition of OPC dispersion is not due to an underlying mobility defect. The *DSCAM*-shRNA-infected OPCs repelled each other similarly to control, indicating DSCAM is dispensable for daughter cell repulsion.

To confirm that PCDH15 plays a key role in OPC daughter cell repulsion, we blocked PCDH15 function by an antibody targeting its extracellular domain (Figure S4C). OPCs were enriched by PDGFRA immunopanning and labeled with *CMV-GFP* adenovirus. Two days after cell transplantation, we applied PCDH15 antibody or control IgG to the cultured brain slices and performed live imaging at DIV3–6. While OPC behavior was normal in the control IgG-treated slices (Figure S4D; Video S6), PCDH15-antibody-treated brain slices resembled *PCDH15* knockdown, with OPC sister cells lingering together long after cell division (Figure S4D; Video S7). These findings indicated PCDH15 function is required for daughter cell separation after OPC division, a behavior that might be important for evenly distributing OPCs across the cortex.

PCDH15 Facilitates OPC Proliferation through Homeostatic Control of OPC Density

As self-avoidance is often closely related to tiling (Hattori et al., 2008), we wondered whether PCDH15 plays a role in OPC tiling, a phenomenon that distributes OPCs in a non-redundant manner to maximize coverage of the surface while minimizing overlap between neighboring OPCs (Hughes et al., 2013). Cultured human cortical slices were incubated with PCDH15 antibody and fixed at DIV7. We labeled OPCs with OLIG2 and O4 to show their nuclei and processes. In comparison with IgG control, PCDH15-antibody-treated slices showed no significant differences in either soma distribution or process arborization (Figure 7A), indicating PCDH15 is not essential for OPC tiling. Furthermore, when we analyzed the time-lapse imaging data of PDGFRA-panned cells, we observed no obvious repulsion between two random OPCs when they encounter each other (Video S8), suggesting PCDH15-mediated repulsion is specific between daughter cells post-division.

Interestingly, many PCDH15-shRNA daughter cells did not reenter the cell cycle, even long after dividing (>40 hr), while the Scramble-control OPCs usually underwent two rounds of division during this same interval. Figure 7B shows one *PCDH15*-shRNA-infected OPC sample that divided to generate two daughter cells close to each other. Instead of both daughter cells dividing to generate four granddaughter cells at a second round of division (Figure 5A; Video S3), only one daughter cell divided to generate two granddaughter cells close to each other, while the other daughter cell remained quiescent (Video S9). This suggested that failure of dispersion of daughter cells might inhibit further division, potentially helping to achieve homeostatic control of local OPC density. To confirm that blocking PCDH15 function affects OPC proliferation, we fixed cultured human cortical slices treated with PCDH15 antibody or control IgG at DIV7 and post-stained with NKX2–2 and KI67. While there was no significant difference in the density of NKX2–2^+ cells between conditions, both number and percentage of NKX2–2^+KI67^+ cells were significantly reduced by incubation with the PCDH15 antibody. Thus, both time-lapse imaging and antibody-blocking experiments support the idea that PCDH15 mediates daughter cell

separation and dispersion, serving to prevent local OPC accumulation and facilitate OPC proliferation.

DISCUSSION

The evolutionary expansion of gray matter has been attributed to a prolonged gestational period as well as the presence of different neural stem cell populations and IPCs that greatly increase the neuronal output of cortical germinal niches. Here, we investigated cellular origins and genetic mechanisms underlying white matter expansion and how oligodendrocyte production is regulated to meet the increased demands for myelination. By combining scRNA-seq, *in vivo* immunohistochemistry, *ex vivo* brain slice culture, and time-lapse imaging, we mapped the lineage trajectory of OPCs from oRGs of the OSVZ in the developing human cortex and identified an intermediate progenitor cell type, we call the $EGFR^+$ Pre-OPC. We also observed enhanced proliferation of embryonic OPCs that helps produce the large number of oligodendrocytes associated with human cortical expansion and described a *PCDH15*-mediated repulsive behavior between OPC daughter cells that promotes dispersal of OPCs and facilitates OPC proliferation. These findings extend our comprehension of human cortical expansion and human oligodendrogenesis.

The Role of oRGs in Human Cortical Oligodendrogenesis

During peak periods of neurogenesis in human cortical development (GW13–19), oRGs populate the OSVZ and produce EOMES-expressing transit-amplifying IPCs that ultimately generate neurons. The abundance of oRGs in primates contributes to the production of large numbers of neurons and provides a secondary radial glia scaffold to support neuronal migration (Lui et al., 2011; Taverna et al., 2014; Fernández et al., 2016; Gertz et al., 2015). However, direct evidence for a possible role of oRGs in gliogenesis is lacking (Rowitch and Kriegstein, 2010). A recent study of the developing macaque suggested that oRGs support oligodendrogenesis but lacked functional validation (Rash et al., 2019), highlighting the need for experimental studies to determine the identity and role of oligodendrocyte progenitors in the developing primate brain. Here, by combining scRNA-seq with functional experiments, we find evidence for oRG-derived OPC generation in the human cerebral cortex. Our study highlights the important role of oRGs for both neurogenesis and gliogenesis. It will be interesting to further compare early neurogenic oRGs with late oligodendrogenic oRGs and study the mechanisms underlying the temporal switch from neurogenesis to oligodendrogenesis.

EGFR-Expressing Intermediate Progenitors and Oligodendrogenesis

EGFR is widely recognized for its importance in cancer, where excessive activation of EGFR signaling often leads to hyper-proliferation of tumor cells (da Cunha Santos et al., 2011; Eskilsson et al., 2018). Here, at the onset of gliogenesis, we find that large numbers of EGFR expressing progenitors occupy germinal zones of the embryonic human cortex and support OPC production. Both lineage reconstruction and differentiation assays indicate that oRGs do not generate OPCs directly; instead, EGFR-expressing cells act as intermediate progenitors for oligodendrogenesis. The existence of proliferative Pre-OPCs in the lineage between oRGs and OPCs may serve to increase rounds of division and enlarge the

progenitor pool size. The responsiveness of Pre-OPCs to EGF suggests a tight regulation of OPC production by EGF secreted in the progenitor cell niche of the developing cortex. Interestingly, we find that a subset of oRGs express *EGF* mRNA in our scRNA-seq database. This suggests a possible mechanism for coordination between neurogenesis and oligodendrogenesis that could serve to match the increase in neuron production to the requirement of more oligodendrocytes for axon myelination. Alternatively, it might represent a positive feedforward mechanism to facilitate OPC production.

Cell Repulsion and Homeostatic Control of OPC Density

In the adult mouse brain, OPCs tile to occupy mutually exclusive territories through a balance between proliferation and self-repulsion, although the molecular mechanisms are unknown (Hughes et al., 2013). In the embryonic human cortex, we observe a self-avoidance behavior between daughter cells following OPC division. This behavior is very different from the phenotype observed in other dividing cells of the developing cortex, including RGs or IPCs, where daughter cells stay in contact long after division (Noctor et al., 2001; Hansen et al., 2010; Betizeau et al., 2013). This is particularly notable when RGs divide asymmetrically to self-renew and generate a neuron, which remains in contact with the parent RG fiber as it migrates. Consecutive divisions of individual RGs and their IPC daughter cells produce a clone of sister cells that remain in contact and eventually form a columnar array of clustered neocortical neurons (Noctor et al., 2001; Yu et al., 2009). In contrast, when OPCs in our study divide symmetrically, the two daughter OPCs strongly repel each other and migrate in opposite directions. This behavior likely serves to avoid local accumulation and ensure broad distribution of OPCs. We find that the mechanism of repulsion involves the protocadherin superfamily member PCDH15 that is selectively enriched in OPCs. According to our differential expression data, DSCAM is also enriched in OPCs, but our functional assays indicate it is not involved in daughter cell repulsion, highlighting the specificity of PCDH15 for OPC dispersion. Furthermore, we observe that failure of daughter cell separation impairs the ability of daughter cells to engage in subsequent divisions, reflecting a cellular mechanism underlying homeostatic control of OPC density during development and highlighting the importance OPC dispersion on OPC proliferation and white matter expansion.

Differential Gene Expression Profile of OPCs

PCDH15 is not only a gene differentially expressed between dividing OPCs and RGs or IPCs but also serves as a marker gene for OPCs. Because our database was composed of most cell types present in the developing human cerebral cortex, including RGs, IPCs, neurons, astrocytes, and microglia, our gene expression database afforded an opportunity to discover marker genes for OPCs. Differential gene expression analysis highlighted several additional cell-type-specific candidate genes, such as *LHFPL3, B3GNT7, LUZP2,* and *SCN1A* (Figure S5A). Future work elucidating the function of these genes in OPC biology may provide insight into human oligodendrocyte development.

OPCs and Cerebral Cortical Malformation

High-throughput sequencing has uncovered a number of gene mutations related to cortical malformations including microcephaly, lissencephaly, and polymicrogyria (Walsh, 1999; Hu

et al., 2014). Although a majority of the gene mutations in patients are germline mutations, most studies of the molecular and cellular mechanisms have focused on the neuronal lineage, while abnormalities in glia have generally not been considered. Our scRNA-seq dataset shows that many genes related to brain malformation are also enriched in OPCs. For example, the microcephaly related genes *ASPM, STIL, CEP135, CDK6, RBBP8, CEP152,* and *CENPJ* are all highly expressed in neuronal progenitors including dividing RGs and IPCs, but they are also highly expressed in dividing OPCs (Figure S5B), suggesting that disease-causing mutations in these genes might also directly interfere with the production of oligodendrocytes and thus contribute to microcephaly. Additionally, our dataset indicates that many polymicrogyria related genes are expressed broadly in both neural progenitors and OPCs, and many of the genes, such as *GPR56, ATP6V0A2, GPSM2, NDE1, RAB18, CCND2, PTEN, DYNC1H1, KIF5C, TUBA1A, TUBB2A, TUBB2B, BICD2, DDX3X, EZH2,* and *OFD1*, show equal or even higher expression levels in OPCs compared with other cell types (Figure S5C). This strongly suggests that an abnormality in OPCs might contribute to polymicrogyria. Together, these cell-type-selective gene expression patterns can inform future analysis of genetic variants associated with neurodevelopmental diseases.

STAR★METHODS

RESOURCE AVAILABILITY

Lead Contact—Further information and requests for resources and reagents for resources and reagents should be directed to and will be fulfilled by the Lead Contact, Arnold R Kriegstein (Arnold.Kriegstein@ucsf.edu).

Material Availability—This study did not generate any new reagents.

Data and Code Availability—Fluidigm C1 and 10x Genomics raw sequencing data were deposited to the database of Genotypes and Phenotypes (dbGaP), accession number phs000989.v4.p1. No custom code was used for the analysis of this data and publicly available algorithm usage is described in the analysis section.

EXPERIMENTAL MODEL AND SUBJECT DETAILS

Embryonic Human Brain Tissue Samples—De-identified tissue samples were collected with previous patient consent in strict observance of the legal and institutional ethical regulations from elective pregnancy termination specimens at San Francisco General Hospital. Protocols were approved by the Human Gamete, Embryo and Stem Cell Research Committee (institutional review board) at the University of California, San Francisco. Human brain tissue was transported to the laboratory within 2h of collection in artificial cerebrospinal fluid containing 125mM NaCl, 2.5mM KCl, 1mM $MgCl_2$, 1mM $CaCl_2$, 1.25mM NaH_2PO_4, 25mm $NaHCO_3$, 25mm D-glucose, bubbled with 95% O_2 and 5% CO_2.

METHOD DETAILS

Immunohistochemistry—Primary tissue samples were cut into 1cm3 pieces and fixed in 4% PFA in Ca^{2+}/Mg2+free PBS (pH = 7.4) for 1h at room temperature or overnight at 4°C with constant agitation. After fixation, they were washed in PBS, equilibrated in 30%

sucrose in PBS overnight at 4°C, embedded in blocks with a 1:1 mixture of 30% sucrose/OCT compound (Tissue-Tek, VWR) and frozen at −80°C. Blocks were frozen sectioned to a thickness of 16–20um cyosections. Antigen retrieval was performed if necessary, by heating section to 95°C in 10mM sodium citrate (pH = 6) for 20min. Sections were then permeablized and blocked with 10% donkey serum in PBS with 0.1% Triton X-100 and 0.2% gelatin. Primary antibody incubations were performed at 4°C overnight, followed by three times of 10min PBS wash, and AlexaFluor secondary antibody (Thermo Fisher, 1:500 dilution) with DAPI incubations were performed at room temperature for 3hr. To detect thymidine analogs (BrdU, CldU or IdU), sections were denatured with 2N HCl for 1hr at room temperature followed by neutralization with 0.1M boric acid, and incubated with primary and secondary antibodies as described above. Slides were mounted with Aqua-mount (Lerner Laboratories). For quantitative analysis of cell numbers in Figures S1, S2, S3, and S4, samples were from 2 to 3 independent biological individuals, and 6 fields of microscrope images from each individual at each position (VZ/ISVZ/OSVZ/IZ/SP/CP) were included. For quantitative analysis of cell numbers in Figure 5B, 10 fields of microscrope images from each individual were included and the experiment was repeated in 3 independent biological individuals.

Primary Cell Dissociation and Immunopanning—Tissue samples were dissected in artificial cerebrospinal fluid using a microsurgical blade under a stereotaxic dissection microscope (Leica). To obtain single cell suspension, tissue samples were further cut into small pieces (< $1mm^3$) and placed in a 6cm dish containing a pre-warmed solution of Papain and DNase freshly diluted in Earl's Balanced Salt Solution that was prepared according to the manufacturer protocol (Worthington Biochemical Corporation). After incubation at 37°C for 1h, tissue was centrifuged at 220 g for 1 min to remove the Papain/DNase supernatant, washed with a OVO protease inhibitor stock solution. After centrifugation at 220 g for 10min, and resuspension in Dulbecco's Modified Eagle Medium / Nutrient Mixture F-12, tissue was further gently triturated by pipetting up and down approximately 10 times into a single cells suspension. The cell suspension was then added to a series of plastic Petri dishes pre-coated with cell-type-specific antibodies and incubated at 37°C for 30min to 1h each. Unbound cells were transferred to the subsequent Petri dish; while the dish with bound cells was rinsed 10 times with DPBS to wash away loosely bound contaminating cell types. Bound cells were digested with 0.05% trypsin/EDTA, centrifuge at 220 g for 15min, and resuspended in corresponding medium.

Primary Cell Culture—Culture chamber slides were prepared by overnight coating with 0.01% poly-L-ornithine (Millipore Sigma) at 37°C. After three water washes, plates were coated with 5ug/ml laminin (Thermo Fisher) and 1ug/ml fibronectin (Corning) for 2hr. Single cell suspension was plated in the culture chamber slides at the concentration of 10^5/well for 8 well chambers or 2×10^5/well for 4 well chambers. Cells were cultured in the medium containing N2 supplement (1:100, Thermo FIsher), B27 supplement (1:50, Thermo Fisher), LIF (20ng/ml, Peprotech), EGF (20ng/ml, Peprotech), Insulin (5ug/ml, Sigma), Penicillin/Streptomycin (100U/ml) in DMEM/F12+GlutamaxTM-I (Thermo Fisher) for the first 2 days, and then in the medium containing N2 supplement, B27 supplement, Insulin, NAC (5ug/ml, Sigma), Biotin (10ng/ml, Sigma), Trace Elements B (1000X, Thermo Fisher),

CNTF (10ng/ml, Pepotech), PDGF (20ng/ml, Peprotech), NT-3 (1ng/ml, Peprotech), Penicillin/Streptomycin (100U/ml) in DMEM/F12+GlutamaxTM-I (Thermo Fisher) for the subsequent 5 or 8 days. Cells were incubated at 37°C, 5% CO_2. For quantitative analysis of cell numbers in Figures 3C and S5C, 5 fields of microscrope images from each individual were included and the experiment was repeated in 3 independent biological individuals.

Primary Organotypic Slice Cultures—Primary tissue samples were cut into 5mm thick pieces, and embedded in 3% low melting point agarose (Thermo Fisher) in artificial cerebrospinal fluid and sectioned into 250um using a Leica VT1200S vibrating blade microtome in artificial cerebrospinal fluid. Slices were then plated on Millicell inserts (Millipore) in the 6-well plate in the medium containing 60% Basal Medium Eagle (Thermo Fisher), 25% Hank's BSS (Thermo Fisher), 10% FBS (Thermo Fisher), 1% Penicillin/Streptomycin/Glutamine (Thermo Fisher), 1% N2 (Thermo Fisher), and 0.66% glucose. Slices were then cultured at 37°C, 5%CO2 and 8% O2 for up to 1 week. For pharmacological treatment assays, EGFR activator EGF was added into the slice culture medium at the final concentration of 50ng/ml [EGF(L)] or 200ng/ml [EGF(H)], while EGFR inhibitors Iressa, AG1478, and PD153035 were added into the slice culture medium at the final concentration of 50nM. For transplantation assays, primary cells were enriched by immunopanning, incubated with CMV-GFP adenovirus for 1hr or shRNA lentivirus for 3hr, washed in DPBS for twice, and injected into the cultured slices using a glass needle pipette. A total of 10^5 cells were evenly injected into 3 pieces of $1cm^2$ brain slices. For thymidine incubation assay, CldU, IdU, or BrdU was added into the slice culture medium at the final concentration of 10nM for 12hr, and three iterations of PBS washing were performed after each thymidine treatment. For quantitative analysis of cell numbers in Figures 3D, 4E, and 7C, 6 fields of microscrope images under each treatment from each individual were included and the experiment was repeated in 3 independent biological individuals.

Time Lapse Image—After 2–3 days culture, GFP-expressing brain slices were transferred into glass-bottom plate with fresh medium, placed to an inverted Leica TCS SP5 with an on-stage incubator streaming 5% CO_2, 8% O_2, balance N_2 into the chamber. Slices were imaged for GFP using a 10X air objective (Zoom 2X) at 35 min intervals for up to 3 or 5 days with repositioning of the z stacks every 24hr. For quantitative analysis in Figures 4D, 6D and 6E, 30 cells from 2–3 independent biological individuals were pooled together.

Single-cell RNA-sequencing—For Fluidigm C1 scRNA-seq, cDNA synthesis and pre-amplification were performed as described before (Nowakowski et al., 2017) using Fluidigm C1 auto-prep system following manufacturer's protocol. After capture, microscope imaging was performed to identify wells with either debris or doublets and retain single-cell wells; these identifications were used in downstream analysis. Library preparation was performed using the llumina Nextera XT library preparation kit. Library concentration quantification was performed using Bioanalyzer (Agilent). Paired-end 100bp sequencing was performed on the Illumina HiSeq2500.

For 10X Genomics scRNA-seq, target capture of 10,000 cells per sample was used; cDNA synthesis, pre-amplification and library preparation were performed as described before (Bhaduri et al., 2020) following manufacturer's protocol "User Guide: Chromium Single

Cell 3′ Reagent Kits (V3 Chemistry).” Libraries from individual samples were pooled and sequenced on the NovaSeq 6000 machine.

Alignment—Trim Galore 3.7 was used to trim 20 bp of adaptor sequencing, and paired-end alignments were performed using HISAT2 to the human reference genome GRCh38. Counts for each cell were performed using subread-1.5.0 function featureCounts. After counts were obtained, normalization to counts per million was performed. Quality control was performed to further ensure that only high quality single cell data was processed further, and cells with fewer than 1000 genes/cell were removed, as were cells with greater than 10% of their individual transcriptome represented in either mitochondrial or ribosomal transcripts. Only genes expressed in at least 30 cells were carried forward in the analysis. For 10X data, the standard Cellranger v3 pipeline was used for alignment and counting.

Single-cell Clustering and Visualization—Principal component analysis (PCA) was used to reduce the dimensionality of the dataset, and clustering was performed as previously described (Shekhar et al., 2016). In PC space, for each cell, the top 30 nearest neighbors were calculated for each cell using the ‘RANN’ R package nn2 function. The Jaccard distance, a weighted distance metric based upon the mutually shared neighbor sets for each pair of neighboring cells was calculated prior to clustering. With the Jaccard weighted distances, louvain clustering was performed using the ‘igraph’ R package. TSNE coordinates were calculated in PCA space (independent of the clusters). Differential expression to identify cluster markers was performed using the FindAllMarkers function in Seurat. The heatmap was generated using key marker genes in the space of a subset of clusters relevant to the analysis. The similarity matrix was calculated by correlating clusters to one another in principal component space. For 10X data, Seurat v3 default clustering parameters were used.

Monocle—Monocle version 2 was used to generate the trajectory analysis. Excitatory neurons, IPCs, RGCs, and OPCs were extracted based upon the above clustering. These cells were re-clustered as above and used as the input to Monocle. Differential gene expression for trajectory construction was performed using these cluster annotations, and metadata of broad cell type was used to color the plot.

shRNA Efficiency Test—HEK293T cells were plated in 12-well plates, and 200ng of cDNA vectors of PCDH15 (NM_001142763.1, Sino Biological HG18931-UT) or DSCAM (NM_001271534.1, Sino Biological HG19944-UT) with 600ng of corresponding shRNA vectors were transfected into the cells using Lipofectamine 3000. Cells were harvested 48 hours after transfection for mRNA extraction using the RNAeasy micro plus kit. RNA quantity and quality were checked using NanoDrop 1000 (Thermo Scientific). qRT-PCR was performed using the ViiA 7 Real-time PCR System with PowerUp SYBR Green Master Mix, and analyzed with comparative Ct method normalized against the housekeeping gene GAPDH. Cells were harvested 72 hours after transfection for protein extraction. Cells were lysed with RIPA buffer (50 mM Tris-HCl pH 8.0, 150 mM NaCl, 1 mM EDTA, 1% NP-40, 0.5% sodium deoxycholate, 0.1% SDS) supplemented with phosphatase and protease inhibitors (Roche). Lysates were homogenized by sonication followed by protein

quantification via BCA assay (Pierce). LDS Sample buffer (Invitrogen) with a reducing agent was added to each lysate followed by a 10 min incubation at 95°C. Samples were spun down and electrophoresed on a 4%–12% Bis-Tris gel, transferred to a nitrocellulose membrane and blocked for one hour with Intercept (TBS) Protein-Free Blocking Buffer (LI-COR) prior to primary antibody incubation o/n. After 1-hour secondary antibody incubation the next day, membranes were imaged using an Odyssey Infrared Imager (LI-COR).

Additionally, OPCs were enriched by PDGFRA-immunopanning and cultured in 12-well plates (for qRT-PCR) or 6-well plate (for western blotting). When the cell density reached 80% of coverage, cells were infected with PCDH15-shRNA or DSCAM-shRNA lentiviruses. OPCs were harvest three days after infection for qRT-PCR, or five days after infection for western blotting.

Antibody Binding Test by FACS—HEK293T cells were seeded into 6-well plates, and 1ug PCDH15 (NM_001142763.1, Sino Biological HG18931-UT), PCDH9 (Dharmacon OHS6085–213579205), or PCHD17 (Dharmacon MHS6278–202801988) cDNA vectors were transfected into the cells using Lipofectamine 3000. For flow cytometry analysis to assay antibody specificity, cells were released 72 hours after cDNA transfection using PBS-EDTA (Lonza). 2 × 10^6 cells per condition were used for PCDH15 primary antibody (R&D systems AF6729, 1:40) staining in FACS staining buffer (D-PBS, 1% BSA, 2mM EDTA, 0.1% sodium azide) for 30 minutes on ice. Next, cells were washed in FACS staining buffer and incubated with Alexa Fluor 488 conjugated secondary antibodies (Invitrogen, 1:400) for 30 minutes on ice. After final washes, Sytox Red (Invitrogen, 1:1000) was added to stain dead cells. Flow cytometry was carried out on an BD LSRFortessa X-20.

QUANTIFICATION AND STATISTICAL ANALYSIS

Quantification of images was performed using the Imaris Image Analysis software (Bitplane). Statistical analysis was performed using Microsoft Excel. Statistical tests, significance values, and experimental n are included in figure legends. All data are shown as mean ± SD. In all cases, p values are represented as follows: ***$p < 0.001$, **$p < 0.01$, *$p < 0.5$, and N.S. when $p > 0.5$.

For quantitative analysis of cell numbers in Figure S1, samples were from 2 to 3 independent biological individuals, and 6 fields of microscrope images from each individual at each position (VZ/ISVZ/OSVZ/IZ/SP/CP) were included. For quantitative analysis of cell numbers in Figures 3C and S2C, 5 fields of microscrope images from each individual were included and the experiment was repeated in 3 independent biological individuals. For quantitative analysis of cell numbers in Figures 3D, 4E, and 7C, 6 fields of microscrope images under each treatment from each individual were included and the experiment was repeated in 3 independent biological individuals. For quantitative analysis of cell numbers in Figure 5B, 10 fields of microscrope images from each individual were included and the experiment was repeated in 3 independent biological individuals. For quantitative analysis in Figures 4D, 6D, and 6E, 30 cells from 2–3 independent biological individuals were pooled together.

Supplementary Material

Refer to Web version on PubMed Central for supplementary material.

ACKNOWLEDGMENTS

We thank Hiroko Nobuta, Manideep Chavali, and Shawn Sorrells for providing resources, suggestions, and technical assistance. Donated tissue samples were obtained in strict compliance with institutional guidelines and ethical oversight. This research was supported by NIH awards P01NS083513 (to D.H.R. and A.R.K.), U01 MH105989, and R01NS075998 (to A.R.K.).

REFERENCES

Barres BA (2014). Designing and troubleshooting immunopanning protocols for purifying neural cells. Cold Spring Harb. Protoc 2014, 1342–1347. [PubMed: 25447277]

Bergles DE, and Richardson WD (2015). Oligodendrocyte development and plasticity. Cold Spring Harb. Perspect. Biol 8, a020453. [PubMed: 26492571]

Betizeau M, Cortay V, Patti D, Pfister S, Gautier E, Bellemin-Ménard A, Afanassieff M, Huissoud C, Douglas RJ, Kennedy H, and Dehay C (2013). Precursor diversity and complexity of lineage relationships in the outer subventricular zone of the primate. Neuron 80, 442–457. [PubMed: 24139044]

Bhaduri A, Andrews MG, Mancia Leon W, Jung D, Shin D, Allen D, Jung D, Schmunk G, Haeussler M, Salma J, et al. (2020). Cell stress in cortical organoids impairs molecular subtype specification. Nature 578, 142–148. [PubMed: 31996853]

Cai J, Qi Y, Hu X, Tan M, Liu Z, Zhang J, Li Q, Sander M, and Qiu M (2005). Generation of oligodendrocyte precursor cells from mouse dorsal spinal cord independent of Nkx6 regulation and Shh signaling. Neuron 45, 41–53. [PubMed: 15629701]

da Cunha Santos G, Shepherd FA, and Tsao MS (2011). EGFR mutations and lung cancer. Annu. Rev. Pathol 6, 49–69. [PubMed: 20887192]

Dugas JC, and Emery B (2013). Purification and culture of oligodendrocyte lineage cells. Cold Spring Harb. Protoc 2013, 810–814. [PubMed: 24003197]

Emery B, and Lu QR (2015). Transcriptional and epigenetic regulation of oligodendrocyte development and myelination in the central nervous system. Cold Spring Harb. Perspect. Biol 7, a020461. [PubMed: 26134004]

Eskilsson E, Røsland GV, Solecki G, Wang Q, Harter PN, Graziani G, Verhaak RGW, Winkler F, Bjerkvig R, and Miletic H (2018). EGFR heterogeneity and implications for therapeutic intervention in glioblastoma. Neurooncol. 20, 743–752.

Fancy SP, Chan JR, Baranzini SE, Franklin RJ, and Rowitch DH (2011). Myelin regeneration: a recapitulation of development? Annu. Rev. Neurosci 34, 21–43. [PubMed: 21692657]

Fernández V, Llinares-Benadero C, and Borrell V (2016). Cerebral cortex expansion and folding: what have we learned? EMBO J. 35, 1021–1044. [PubMed: 27056680]

Fietz SA, Kelava I, Vogt J, Wilsch-Bräuninger M, Stenzel D, Fish JL, Corbeil D, Riehn A, Distler W, Nitsch R, and Huttner WB (2010). OSVZ progenitors of human and ferret neocortex are epithelial-like and expand by integrin signaling. Nat. Neurosci 13, 690–699. [PubMed: 20436478]

Fish JL, Dehay C, Kennedy H, and Huttner WB (2008). Making bigger brains-the evolution of neural-progenitor-cell division. J. Cell Sci 121, 2783–2793. [PubMed: 18716282]

Fogarty M, Richardson WD, and Kessaris N (2005). A subset of oligodendrocytes generated from radial glia in the dorsal spinal cord. Development 132, 1951–1959. [PubMed: 15790969]

Freeman MR, and Rowitch DH (2013). Evolving concepts of gliogenesis: a look way back and ahead to the next 25 years. Neuron 80, 613–623. [PubMed: 24183014]

Fuerst PG, Koizumi A, Masland RH, and Burgess RW (2008). Neurite arborization and mosaic spacing in the mouse retina require DSCAM. Nature 451, 470–74. [PubMed: 18216855]

Gertz CC, and Kriegstein AR (2015). Neuronal migration dynamics in the developing ferret cortex. J. Neurosci. 35, 14307–14315. [PubMed: 26490868]

Hansen DV, Lui JH, Parker PR, and Kriegstein AR (2010). Neurogenic radial glia in the outer subventricular zone of human neocortex. Nature 464, 554–561. [PubMed: 20154730]

Hattori D, Millard SS, Wojtowicz WM, and Zipursky SL (2008). Dscam-mediated cell recognition regulates neural circuit formation. Annu. Rev. Cell Dev. Biol 24, 597–620. [PubMed: 18837673]

Hill RA, Patel KD, Goncalves CM, Grutzendler J, and Nishiyama A (2014). Modulation of oligodendrocyte generation during a critical temporal window after NG2 cell division. Nat. Neurosci 17, 1518–1527. [PubMed: 25262495]

Hu WF, Chahrour MH, and Walsh CA (2014). The diverse genetic landscape of neurodevelopmental disorders. Annu. Rev. Genomics Hum. Genet 15, 195–213. [PubMed: 25184530]

Hughes EG, Kang SH, Fukaya M, and Bergles DE (2013). Oligodendrocyte progenitors balance growth with self-repulsion to achieve homeostasis in the adult brain. Nat. Neurosci 16, 668–676. [PubMed: 23624515]

Jakovcevski I, and Zecevic N (2005). Sequence of oligodendrocyte development in the human fetal telencephalon. Glia 49, 480–491. [PubMed: 15578660]

Kessaris N, Fogarty M, lannarelli P, Grist M, Wegner M, and Richardson WD (2006). Competing waves of oligodendrocytes in the forebrain and postnatal elimination of an embryonic lineage. Nat. Neurosci 9, 173–179. [PubMed: 16388308]

Lefebvre JL, Kostadinov D, Chen WV, Maniatis T, and Sanes JR (2012). Protocadherins mediate dendritic self-avoidance in the mammalian nervous system. Nature 488, 517–521. [PubMed: 22842903]

Lui JH, Hansen DV, and Kriegstein AR (2011). Development and evolution of the human neocortex. Cell 146, 18–36. [PubMed: 21729779]

Marques S, Zeisel A, Codeluppi S, van Bruggen D, Mendanha Falcão A, Xiao L, Li H, Häring M, Hochgerner H, Romanov RA, et al. (2016). Oligodendrocyte heterogeneity in the mouse juvenile and adult central nervous system. Science 352, 1326–1329. [PubMed: 27284195]

Marques S, van Bruggen D, Vanichkina DP, Floriddia EM, Munguba H, Väremo L, Giacomello S, Falcão AM, Meijer M, Björklund AK, et al. (2018). Transcriptional convergence of oligodendrocyte lineage progenitors during development. Dev. Cell 46, 504–517.e7. [PubMed: 30078729]

Mo Z, and Zecevic N (2009). Human fetal radial glia cells generate oligodendrocytes in vitro. Glia 57, 490–498. [PubMed: 18814269]

Noctor SC, Flint AC, Weissman TA, Dammerman RS, and Kriegstein AR (2001). Neurons derived from radial glial cells establish radial units in neocortex. Nature 409, 714–720. [PubMed: 11217860]

Nonaka-Kinoshita M, Reillo I, Artegiani B, Martínez-Martínez MA, Nelson M, Borrell V, and Calegari F (2013). Regulation of cerebral cortex size and folding by expansion of basal progenitors. EMBO J. 32, 1817–1828. [PubMed: 23624932]

Nowakowski TJ, Bhaduri A, Pollen AA, Alvarado B, Mostajo-Radji MA, Di Lullo E, Haeussler M, Sandoval-Espinosa C, Liu SJ, Velmeshev D, et al. (2017). Spatiotemporal gene expression trajectories reveal developmental hierarchies of the human cortex. Science 358, 1318–1323. [PubMed: 29217575]

Pollen AA, Nowakowski TJ, Chen J, Retallack H, Sandoval-Espinosa C, Nicholas CR, Shuga J, Liu SJ, Oldham MC, Diaz A, et al. (2015). Molecular identity of human outer radial glia during cortical development. Cell 163, 55–67. [PubMed: 26406371]

Pringle NP, and Richardson WD (1993). A singularity of PDGF alpha-receptor expression in the dorsoventral axis of the neural tube may define the origin of the oligodendrocyte lineage. Development 117, 525–533. [PubMed: 8330523]

Qiu X, Mao Q, Tang Y, Wang L, Chawla R, Pliner HA, and Trapnell C (2017). Reversed graph embedding resolves complex single-cell trajectories. Nat. Methods 14, 979–982. [PubMed: 28825705]

Rakic S, and Zecevic N (2003). Early oligodendrocyte progenitor cells in the human fetal telencephalon. Glia 41, 117–127. [PubMed: 12509802]

Rash BG, Duque A, Morozov YM, Arellano JI, Micali N, and Rakic P (2019). Gliogenesis in the outer subventricular zone promotes enlargement and gyrification of the primate cerebrum. Proc. Natl. Acad. Sci. USA 116, 7089–7094. [PubMed: 30894491]

Rowitch DH, and Kriegstein AR (2010). Developmental genetics of vertebrate glial-cell specification. Nature 468, 214–222. [PubMed: 21068830]

Simons M, and Nave KA (2015). Oligdendrocytes, Myelination and axonal support. Cold Spring Harb. Perspect. Biol 8, a020479. [PubMed: 26101081]

Smart IH, Dehay C, Giroud P, Berland M, and Kennedy H (2002). Unique morphological features of the proliferative zones and postmitotic compartments of the neural epithelium giving rise to striate and extrastriate cortex in the monkey. Cereb. Cortex 12, 37–53. [PubMed: 11734531]

Subramanian L, Bershteyn M, Paredes MF, and Kriegstein AR (2017). Dynamic behaviour of human neuroepithelial cells in the developing forebrain. Nat. Commun 8, 14167. [PubMed: 28139695]

Taverna E, Götz M, and Huttner WB (2014). The cell biology of neurogenesis: toward an understanding of the development and evolution of the neocortex. Annu. Rev. Cell Dev. Biol 30, 465–502. [PubMed: 25000993]

Trapnell C, Cacchiarelli D, Grimsby J, Pokharel P, Li S, Morse M, Lennon NJ, Livak KJ, Mikkelsen TS, and Rinn JL (2014). The dynamics and regulators of cell fate decisions are revealed by pseudotemporal ordering of single cells. Nat. Biotechnol 32, 381–386. [PubMed: 24658644]

Vallstedt A, Klos JM, and Ericson J (2005). Multiple dorsoventral origins of oligodendrocyte generation in the spinal cord and hindbrain. Neuron 45, 55–67. [PubMed: 15629702]

Walsh CA (1999). Genetic malformations of the human cerebral cortex. Neuron 23, 19–29. [PubMed: 10402190]

Warf BC, Fok-Seang J, and Miller RH (1991). Evidence for the ventral origin of oligodendrocyte precursors in the rat spinal cord. J. Neurosci 11, 2477–2488. [PubMed: 1869925]

Yu YC, Bultje RS, Wang X, and Shi SH (2009). Specific synapses develop preferentially among sister excitatory neurons in the neocortex. Nature 458, 501–504. [PubMed: 19204731]

Zecevic N, Chen Y, and Filipovic R (2005). Contributions of cortical subventricular zone to the development of the human cerebral cortex. J. Comp. Neurol 491, 109–122. [PubMed: 16127688]

Zhang K, and Sejnowski TJ (2000). A universal scaling law between gray matter and white matter of cerebral cortex. Proc. Natl. Acad. Sci. USA 97, 5621–5626. [PubMed: 10792049]

Zhu X, Hill RA, Dietrich D, Komitova M, Suzuki R, and Nishiyama A (2011). Age-dependent fate and lineage restriction of single NG2 cells. Development 138, 745–753. [PubMed: 21266410]

Highlights

- Human oRGs are a novel source of EGFR^{+} Pre-OPCs
- Pre-OPCs undergo diminutive MST during division
- Human OPC proliferation exponentially increases the progenitor pool
- OPC-enriched PCDH15 regulates daughter cell repulsion and proliferation

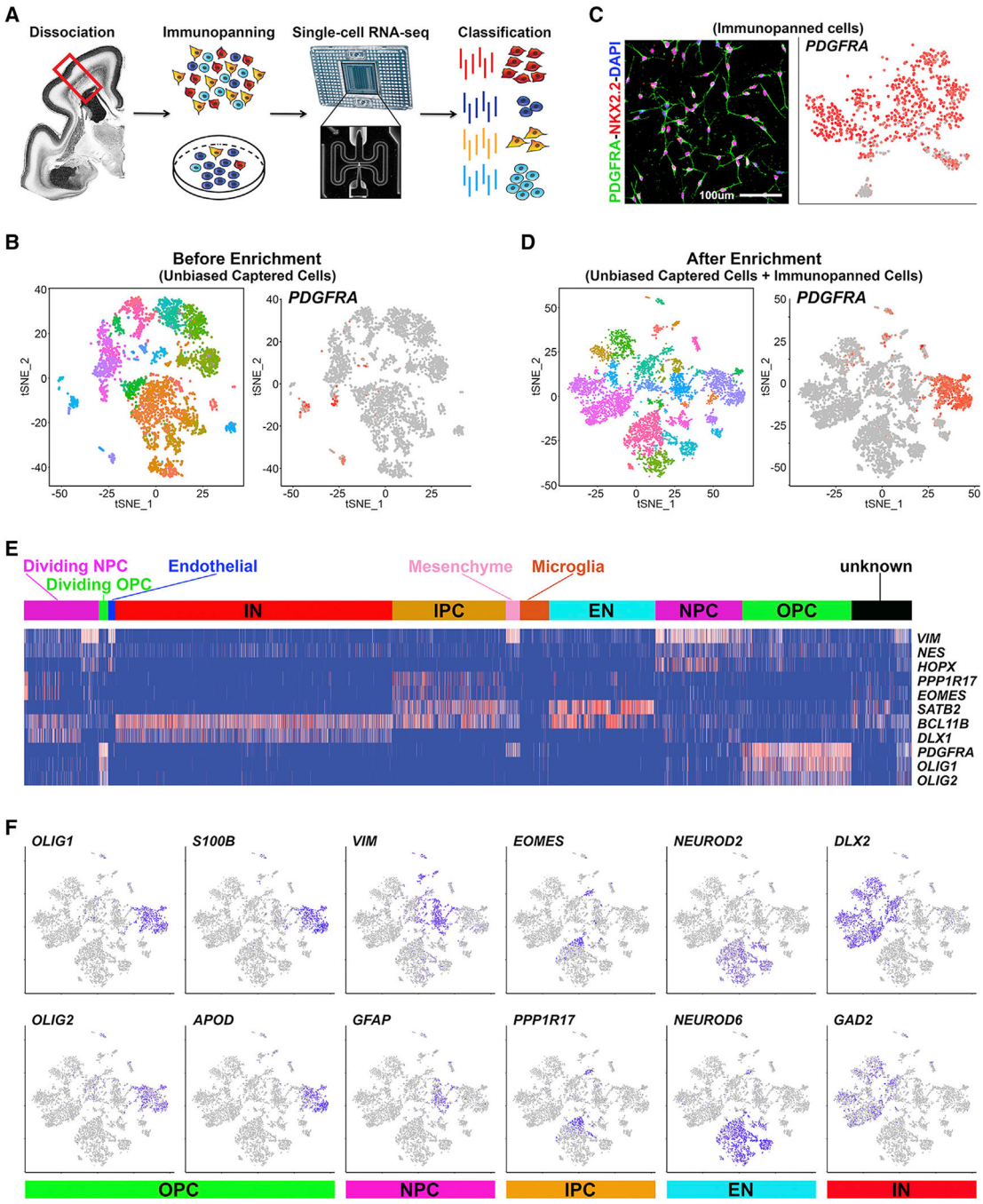

Figure 1. scRNA-seq of OPCs from the Developing Human Cortex

(A) Schematic of the workflow. Developing human cortex was dissociated and OPCs enriched by PDGFRA immunopanning. Single cells were isolated using the Fluidigim C1 microfluidic chip system, and pair-end single-cell RNA sequencing (scRNA-seq) was performed. Clustering was used to annotate cell types according to RNA profiles.

(B) Scatterplot by t-stochastic neighbor embedding (tSNE) (left) and feature plot of *PDGFRA*-mRNA expression (right) from Nowakowski et al. (2017).

(C) Validation of the immunopanning strategy by immunostaining or scRNA-seq.

(D) Scatterplot by tSNE (left) and feature plot of *PDGFRA*-mRNA expression (right) of data generated by immunopanning in this study with Nowakowski et al. (2017).
(E) Heatmap showing cluster annotations and marker gene expression.
(F) Feature plots of marker genes of different cell types.

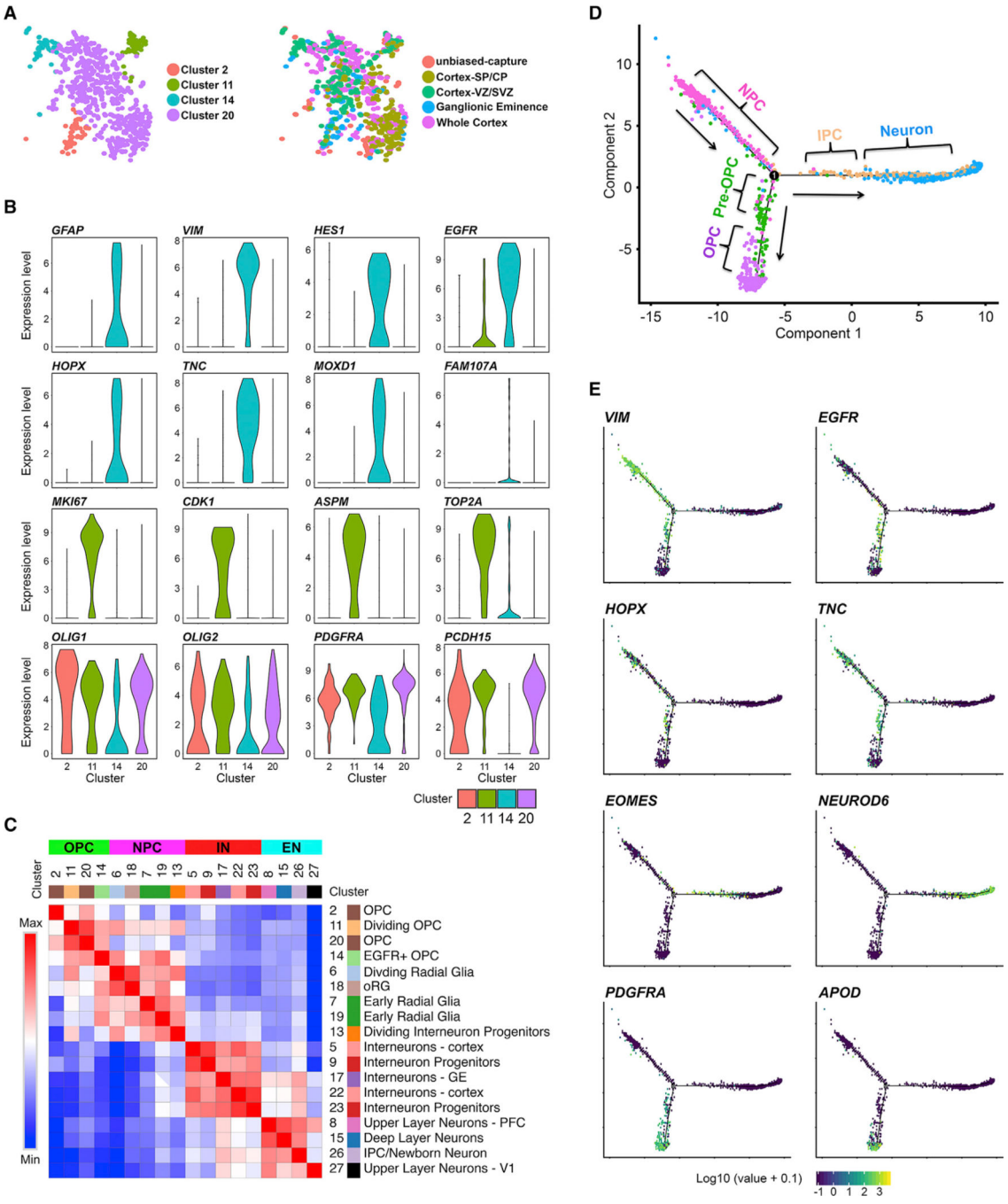

Figure 2. Characterization of OPC Clusters from scRNA-seq

(A) Enlarged tSNE plot from Figure 1D focusing on the OPC clusters. Clusters are shown on the left, and metadata annotation of tissue source is represented on the right.

(B) Violin plots of differentially expressed genes in OPC clusters.

(C) Similarity matrix of OPC, NPC, and neuronal clusters.

(D) Trajectory analysis of progenitor and OPC cell types using Monocle. Broad cell types are shown rather than individual clusters.

(E) Feature plots of marker genes for NPCs, IPCs, neurons, and OPCs indicating lineage progression.

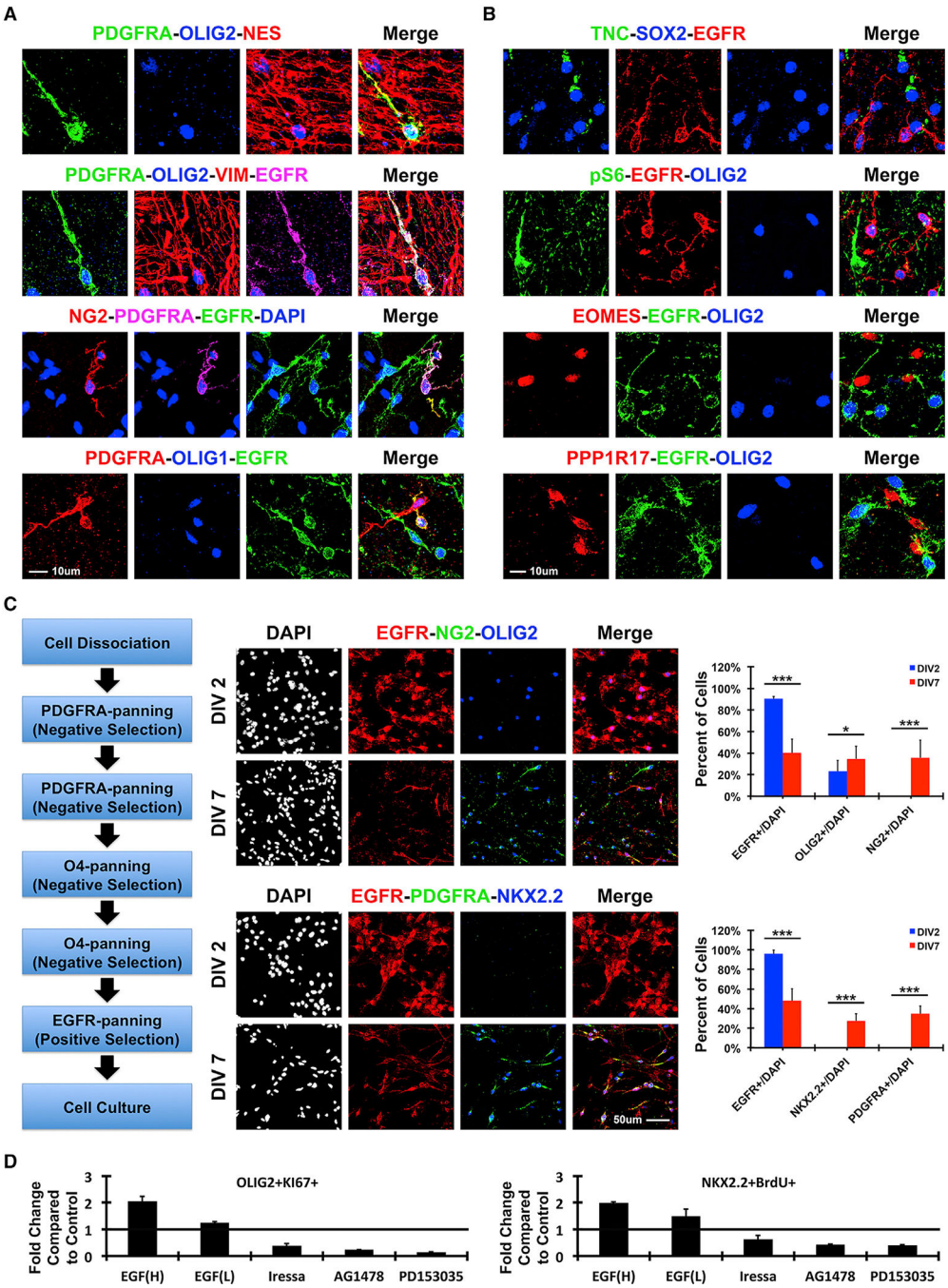

Figure 3. EGFR-Expressing Progenitors Generate OPCs in the Developing Human Cortex

(A) Characterization of Pre-OPCs that co-express NPC and OPC markers. Images are from human OSVZ at GW20–24 (n = 12).

(B) Characterization of EGFR-expressing progenitors by oRG or IPC marker co-staining. Images are from human OSVZ at GW20–24 (n = 12).

(C) Outline of immunopanning workflow (left). Images of marker staining at DIV2 and DIV7 showing lineage progression (middle). Quantification of cell proportions (right). Mean ± SD (n = 5). (***p < 0.001; **p < 0.01; *p < 0.05; N.S., p > 0.05.)

(D) Quantification of dividing OPCs in cultured human brain slices after pharmacologically activating [EGF(High) and EGF(Low)] or inhibiting (Iressa, AG1478, and PD153035) EGFR. Mean ± SD (n = 6).

See also Figures S1 and S2.

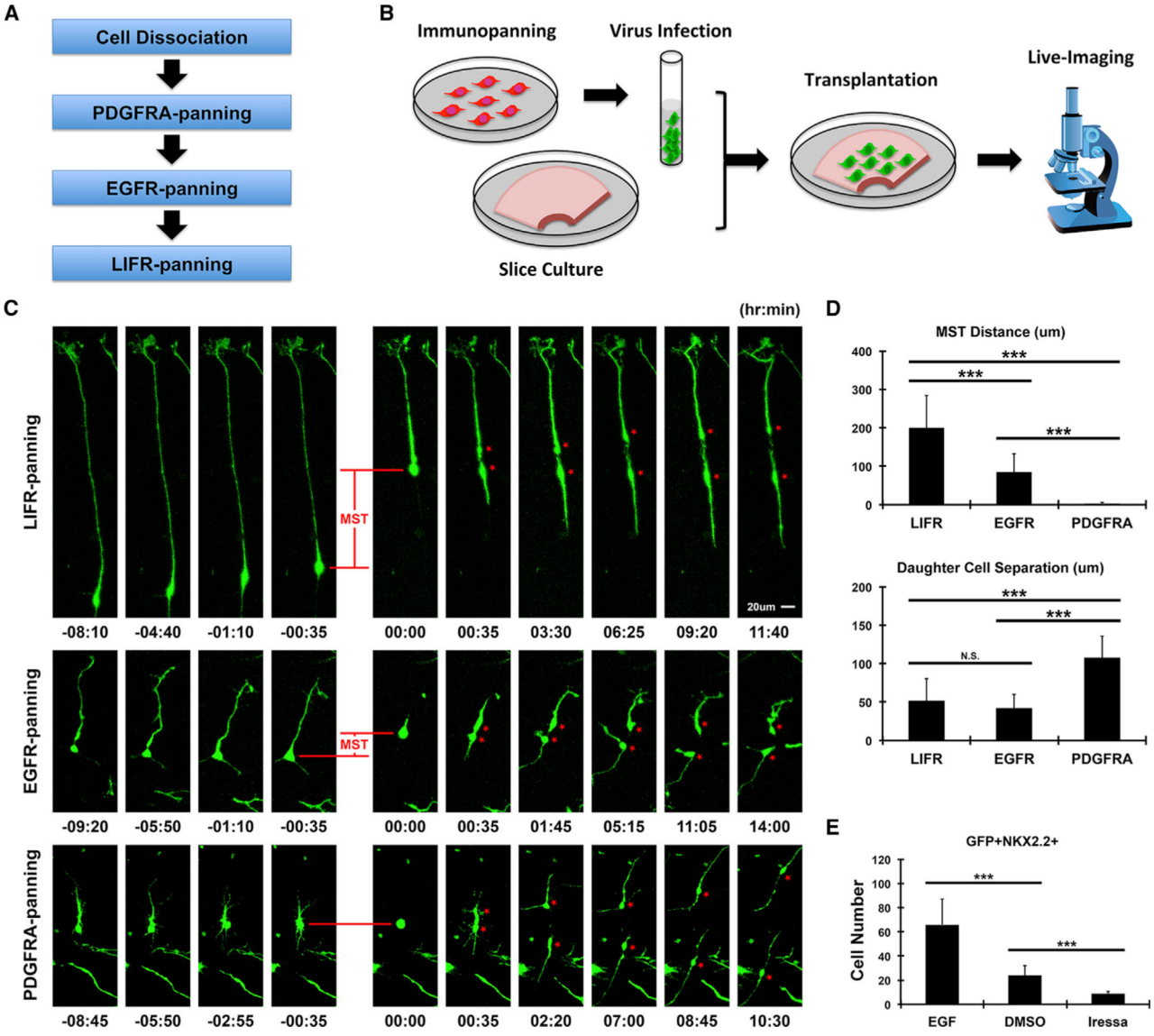

Figure 4. Characterization of Division Dynamics of EGFR-Expressing Progenitors in the Developing Human Cortex

(A) Outline of immunopanning workflow. Different types of progenitors in the OSVZ were positively selected with PDGFRA, EGFR, and LIFR antibodies by sequential immunopanning.

(B) Schematic of the experimental strategy. Progenitors were enriched by immunopanning, infected with GFP adenovirus, injected into cultured cortical slices, and observed for time-lapse imaging.

(C) Time-stamped still images of dividing progenitors enriched by LIFR, EGFR, or PDGFRA panning. Representative cells from cultured cortical slices at GW20–24 (n = 30).

(D) Quantification of MST distance during division and daughter cell separation of different progenitors at 6 hr after division. Mean ± SD (n = 30). (***p < 0.001; N.S., p > 0.05.)

(E) Quantification of OPCs from EGFR-panned cells in cultured human brain slices after pharmacologically activating (EGF) or inhibiting (Iressa) EGFR. Mean ± SD (n = 6). (***p < 0.001.)

See also Figure S3 and Videos S1 and S2.

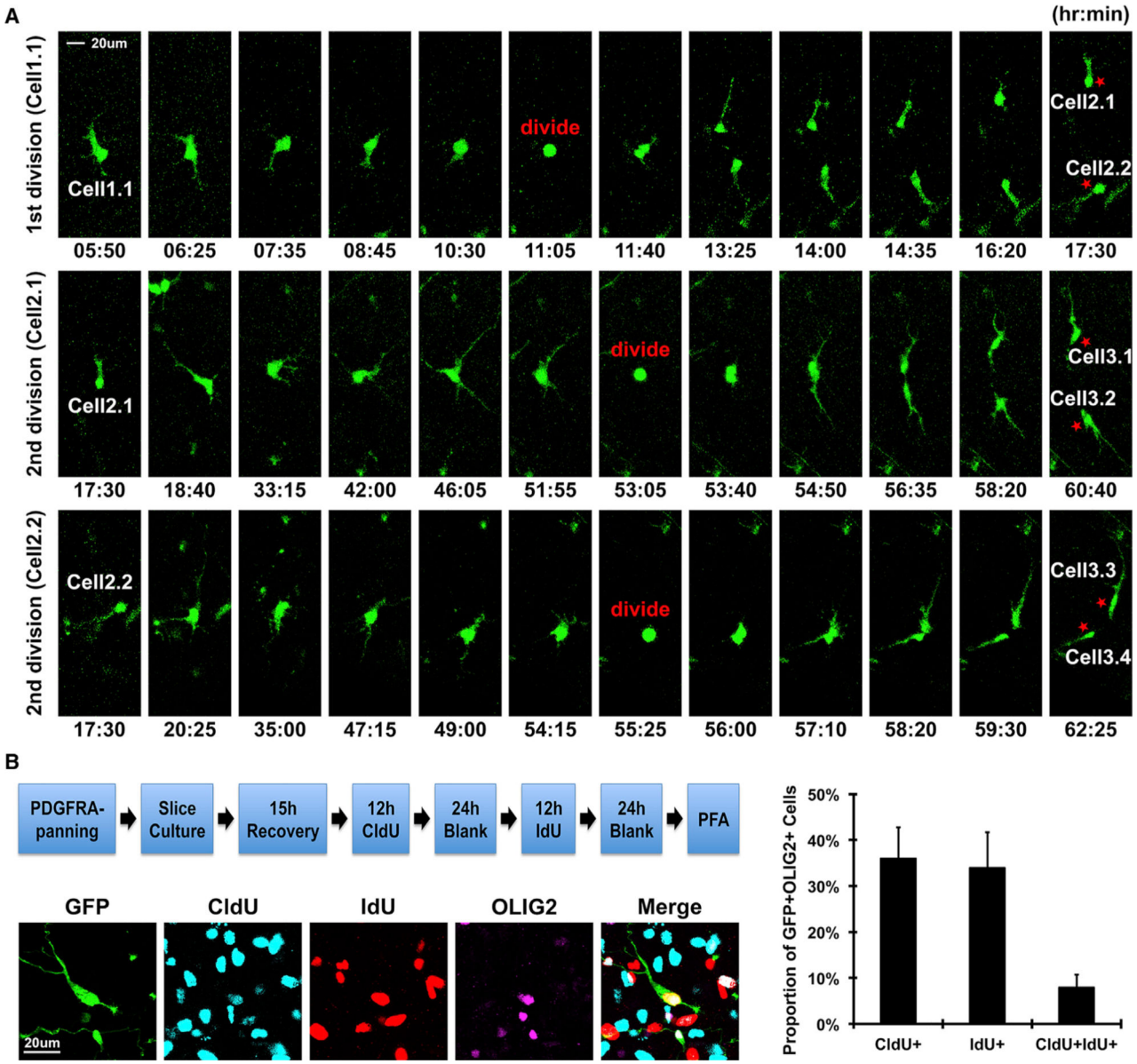

Figure 5. Characterization of Division Properties of Human Embryonic OPCs

(A) Time-stamped still images of dividing OPCs. Two rounds of continuous division were observed and four granddaughter cells were generated. Representative cell from a cultured cortical slice at GW22 (n = 20).

(B) Workflow to explore OPC division quantitatively (top left). OPCs were enriched with PDGFRA immunopanning, infected with GFP adenovirus before transplantation and thymidine analog labeling. Representative images show a GFP-positive immunopanned cell co-labeled with CldU and IdU and expressing OLIG2 (bottom left) (n = 20). Quantification of the proportion of $GFP^{+}OLIG2^{+}$ cells that express either CldU or IdU or both on cultured cortical slices (n = 10). Mean ± SD (right).

See also Video S3.

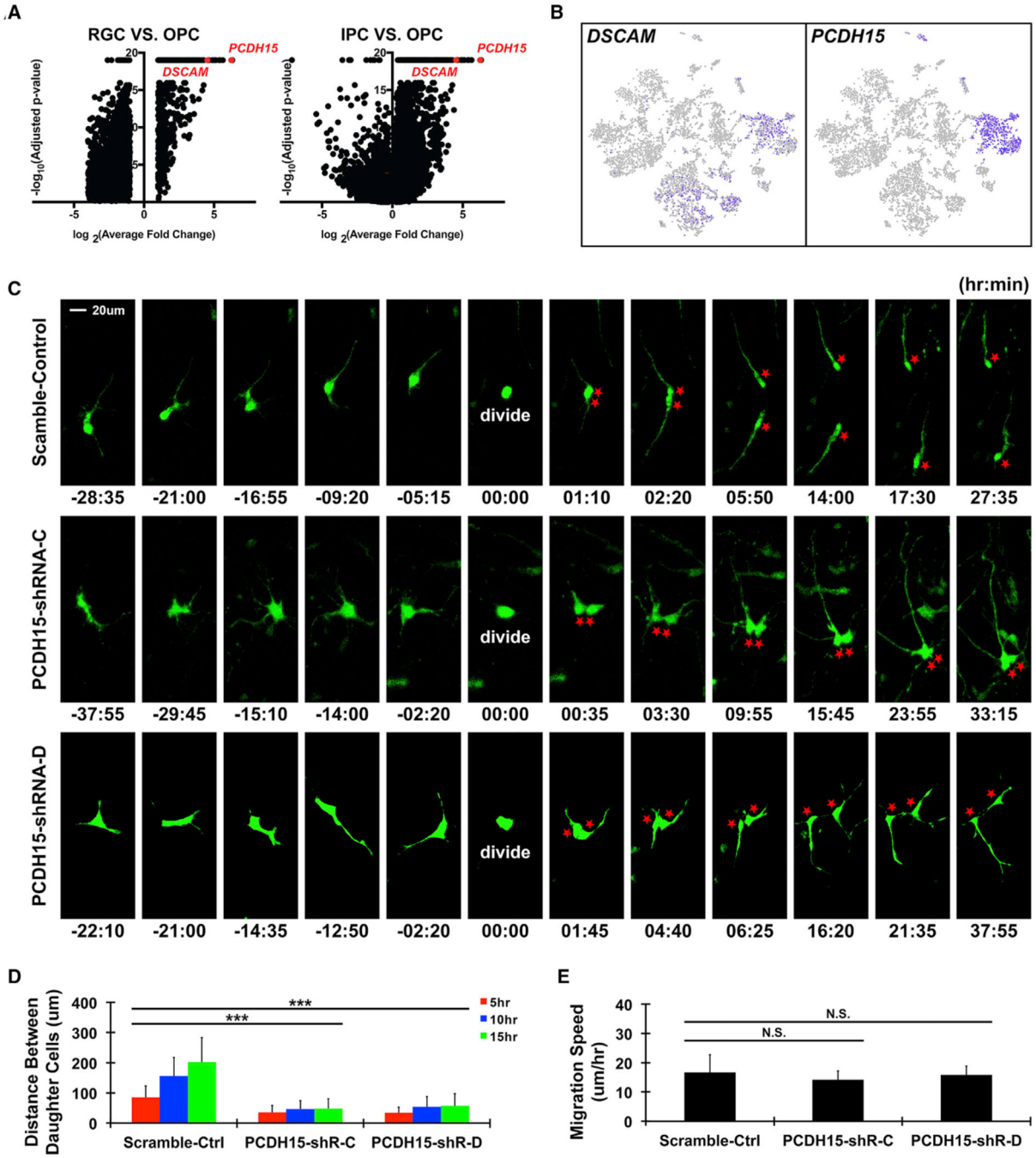

Figure 6. PCDH15 Mediates Daughter Cell Repulsion after OPC Division

(A) Volcano plots show differentially expressed genes between dividing OPCs and dividing RGs (left) or dividing IPCs (right). Two of the most highly differentially expressed genes are *DSCAM* and *PCDH15.*

(B) Feature plots of *DSCAM* (left) shows expression in INs and OPCs, while *PCDH15* is specific to OPCs.

(C) Time-stamped still images of dividing OPCs treated with either scramble-shRNA control lentiviruses or *PCDH15*-shRNA lentiviruses. Representative cells are from cultured cortical slices at GW20–24 (n = 30).

(D) Quantification of daughter cell distance after division. Mean ± SD (n = 30). (***p < 0.001.)

(E) Quantification of migration speed before division. Mean ± SD (n = 30). (N.S., p > 0.05.)

See also Figure S4 and Videos S4, S5, S6, and S7.

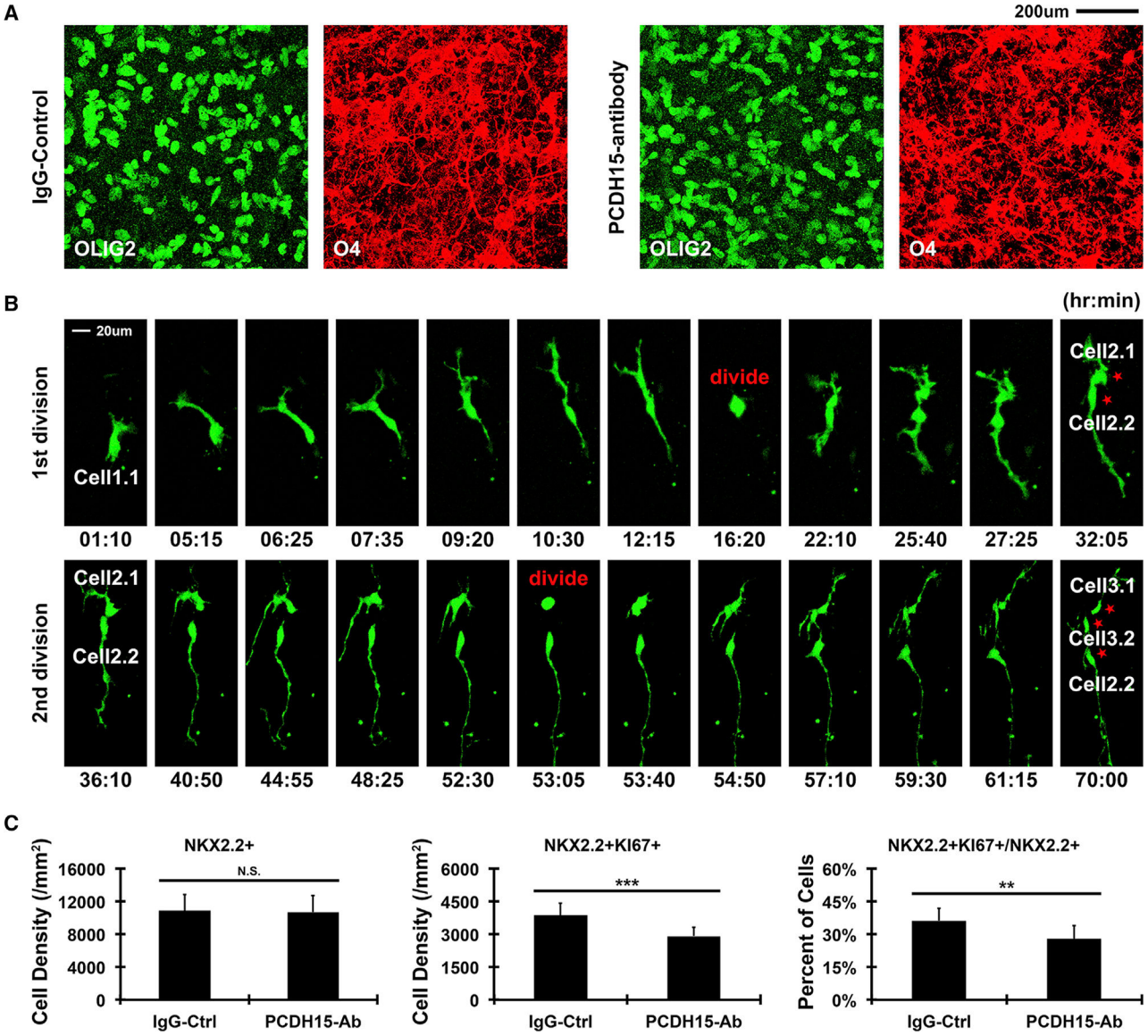

Figure 7. Interfering with PCDH15 Function Affects OPC Proliferation

(A) Sample images of OPCs in the OSVZ of cultured brain slices treated with either IgG as control or PCDH15 antibody to interfere with PCDH15 function. Blocking to PCDH15 function did not cause obvious change in OPC morphology (O4 staining) and distribution (OLIG2 staining).

(B) Time-stamped still images of dividing OPCs infected with *PCDH15*-shRNA lentiviruses. Two rounds of continuous division were observed, and only one of the daughter cells divided again. Representative cells are from cultured cortical slices at GW20–24 (n = 6).

(C) Quantification of OPC division in the OSVZ of cultured brain slices treated with either IgG or PCDH15 antibody. Blocking to PCDH15 function inhibited OPC proliferation but did not change local OPC density. Mean ± SD (n = 6). (***p < 0.001; **p < 0.01; N.S., p > 0.05.)

See also Videos S8 and S9.

KEY RESOURCES TABLE

REAGENT or RESOURCE	SOURCE	IDENTIFIER
Antibodies		
Mouse monoclonal anti-PDGFRA	BD Biosciences	Cat.# 556001
Mouse monoclonal anti-O4	Millipore	Cat.# MAB345
Rat monoclonal anti-EGFR	Abcam	Cat.# ab231
Mouse monoclonal anti-LIFR	Abcam	Cat.# ab89792
Donkey anti-Mouse IgG	Jackson Immunoresearch	Cat.# 715-005-151
Donkey anti-Mouse IgM	Jackson Immunoresearch	Cat.# 715-005-020
Goat anti-Rat IgG	Jackson Immunoresearch	Cat.# 112-005-003
Rabbit anti-PDGFRA, 1:500	Cell Signaling	Cat.# 3174S
Mouse anti-PDGFRA, 1:200	BD Biosciences	Cat.# 556001
Goat anti-PDGFRA, 1:500	R&D Systems	Cat.# AF-307-NA
Rabbit anti-NG2, 1:100	Millipore	Cat.# AB5320
Rabbit anti-OLIG2, 1:500	Millipore	Cat.# AB9610
Mouse anti-OLIG2, 1:200	Millipore	Cat.# MABN50
Goat anti-OLIG2, 1:200	R&D Systems	Cat.# AF2418
Mouse anti-NKX2-2, 1:200	Abcam	Cat.# ab187375
Rabbit anti-EGFR, 1:500	Abcam	Cat.# ab32077
Sheep anti-EGFR, 1:500	Abcam	Cat.# ab98133
Mouse anti-SOX2, 1:300	BD Biosciences	Cat.# 561506
Goat anti-SOX2, 1:300	Santa Cruz	Cat.# sc-17320
Rabbit anti-PTPRZ1, 1:500	Atlas Antibodies	Cat.# HPA015103
Mouse anti-TNC, 1:100	Santa Cruz	Cat.# sc-25328
Rabbit anti-HOPX, 1:500	Proteintech	Cat.# 11419-1-AP
Rabbit anti-pS6, 1:300	Cell Signaling	Cat.# 2211S
Mouse anti-NES, 1:200	Millipore	Cat.# MAB5326
Rat anti-GFAP, 1:1000	Invitrogen	Cat.# 13-0300
Chicken anti-VIM, 1:1000	Millipore	Cat.# AB5733
Mouse anti-pVIM (Ser55), 1:500	MBL	Cat.# D076-3
Mouse anti-pVIM (Ser82), 1:500	MBL	Cat.# D095-3
Sheep anti-EOMES, 1:300	R&D Systems	Cat.# AF6166
Rabbit anti-PPP1R17, 1:300	Atlas Antibodies	Cat.# HPA047819
Mouse anti-KI67, 1:200	Dako	Cat.# M7240
Chicken anti-GFP, 1:1000	Abcam	Cat.# ab13970
Rat anti-BrdU (CldU), 1:500	BIO-RAD	Cat.# OBT0030G
Mouse anti-ldU, 1:200	Sigma-Aldrich	Cat.# SAB3701448
Sheep anti-PCDH15	Invitrogen	Cat.# PA5-47865
Bacterial and Virus Strains		
CMV-GFP adenovirus	Vector Biolabs	Cat. # 1060

REAGENT or RESOURCE	SOURCE	IDENTIFIER
PCDH15-shRNA lenti-virus	Origene	Cat.# TL302649V
DSCAM-shRNA lenti-virus	Origene	Cat.# TL304905V
Chemicals, Peptides, and Recombinant Proteins		
Iressa	Tocris	Cat.# 3000
AG1478	Tocris	Cat.# 1276
PD153035	Tocris	Cat.# 1037
LIF	Peprotech	Cat.# 300-05
EGF	Peprotech	Cat.# 100-47
PDGF	Peprotech	Cat.# 100-13A
CNTF	Peprotech	Cat.# 450-13
NT-3	Peprotech	Cat.# 450-03
Critical Commercial Assays		
C1 Single-Cell Auto Prep Integrated Fluidic Circuit	Fluidigm	N/A
SMARTer Ultra Low RNA Kit	Clontech	Cat.# 634848
Chromium Chip v3 Single Cell Kit	10X Genomics	Cat.# PN-1000092
Nextera XT DNA Sample Preparation Kit	Illumina	Cat.# FC-131-1096
Deposited Data		
Single-cell RNA-sequencing Data	This paper	phs000989.v4.p1